CMD5 Table 1 Comparison of Measured and Calculated Limits L_{max}/ℓ_s in Reflection and Transmission (The model tends to overestimate the ability of the confocal microscope to suppress diffuse light.)

	ℓ_s (μm)	Δz (mm)	L_{max}/ℓ_s measured	L_{max}/ℓ_s calculated
reflection	460	1.3	12	13
NA=0.28	220	3.8	16	16
transmission	6	0	5	5
NA=0.12	6	2.5	9	10
	190	0	10	15
	190	12.5	11	16

back side (transmission geometry) of the sample with respect to the focus Δz, provided that L/ℓ_s is constant. It is approximately independent of the distance between the collector lens and the spatial filter, z, and improves with the square of the numerical aperture (NA). Figure 2 shows the value L_{max}/ℓ_s for which the ratio becomes unity. The calculated ratio is compared with measurements in reflection and transmission in Table 1.

It turns out that the heterodyne detection suppresses diffuse light by a factor of $1/\sqrt{N}$ as compared with the confocal setup where N is the number of mutually incoherent speckle spots on the detector. Because N is inversely proportional to the distance z squared, placing the detector as close as possible to the collector lens is expected to yield optimum suppression of diffuse light using heterodyne mixing. We will show that this is indeed the case. For a typical setup, one can achieve a reduction of the diffuse light by two orders of magnitude. This allows one to extend the maximum sample thickness for ballistic imaging by about five mean free paths. For human dermis (ℓ = 0.3 mm, ℓ_s = 0.05 mm at 633 nm), for example, we obtain a limit of confocal imaging with NA = 0.3 of about L_{max} = 0.8 mm which can be extended to L = 1.1 mm using heterodyne detection with narrow bandwidth light.

*New York State Center for Advanced Technology for Ultrafast Photonic Materials and Applications, Department of Physics, Queens College of the City University of New York, 65-30 Kissena Blvd., Flushing, New York 11367

1. *Handbook of Biological Confocal Microscopy*, E. J. Pawley, Ed., Plenum Press, New York (1990).
2. See, e.g., *Advances in Optical Imaging and Photon Migration*, R. R. Alfano, Ed. Vol. 21, OSA Proceedings Series (Optical Society of America, Washington, DC, 1994).
3. M. Kempe, W. Rudolph, Opt. Lett. **19**, 1919–1921 (1994).
4. M. Kempe, W. Rudolph, E. Welsch, in J. Opt. Soc. Am. A **13** (1996).
5. K. Takada, I. Yokohama, K. Chida, J. Noda, Appl. Opt. **26**, 1603–1606 (1987).

CMD6 **9:30 am**

Spatial resolution limit of time-gated imaging through random scattering media

Hai-Pang Chiang, Jyhpyng Wang, *Institute of Atomic and Molecular Sciences, Academia Sinica and Department of Electrical Engineering, National Taiwan University, P.O. Box 23-166, Taipei, Taiwan*

Recently various time-gating techniques have been applied to imaging through random scattering media, in particular animal tissues. Because scattered photons travel longer paths, by time-gating one can reject scattered photons, thereby reducing interferences from scattering. An interesting question about time-gated imaging through random scattering media is the limit of spatial resolution. Because the gating width cannot be infinitesimally small, it is not clear how parameters such as the gating width and the medium thickness determine the resolution or, furthermore, in what way the image degrades as the object size becomes smaller than the resolution limit. To answer these questions, we analyze spatial distributions of time-gated photons, which have traveled through random scattering media, by a method at random-phase path integration and from the distributions we derive the resolution limit.

In random scattering media photons follow zig-zag paths with a scattering-angle distribution approximated by $P(\theta) = 1 + 3g\cos(\theta)$, where g is a parameter representing the anisotropy of the distribution. We may calculate the probability of any particular zig-zag path by applying $P(\theta)$ repetitively for all the scattering positions on the path. Then by integrating all possible paths whose lengths are within the gating window, we obtain the gated photon distribution at the exit plane. As a first-order approximation, we consider paths which has been scattered only once, as shown in Fig. 1, and leave multiply scattered paths as correction terms. It turns out that multiply scattered paths have negligible influence on the resolution because most of them fall out of the gating window. The relative phases among the paths are assumed to be random, therefore, we only need to count photons at every output positions. This is why we call the method random-phase path integration. The model we used in the calculation is an opaque wire in a random scattering medium, which corresponds closely to our previous time-gated imaging experiments.[1,2] Under the practical condition $w \ll r \ll L \leq D$, where w is the width of the gating window, r the radius of the wire, L the distance of the wire from the exit plane, and D the thickness of the medium, we can calculate the gated photon distribution analytically.

Figure 2 shows a calculated photon distribution compared with experimental

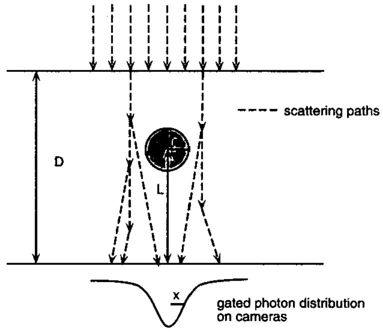

CMD6 Fig. 1 Model of analyses. (r: radius of the hidden object; D: thickness of the medium; L: distance of the object from the exit plane; w: width of the gating window.)

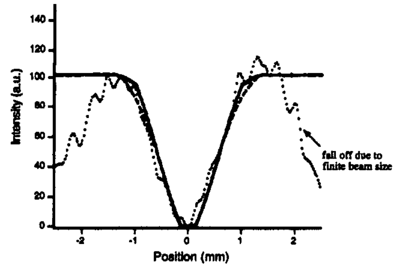

CMD6 Fig. 2 Time-gated photon distributions. Solid line: random-phase path integration; dashed line: Monte Carlo simulation; dot: experimental data. D = 8 mm, L = 4 mm, w = 40 μm, r = 0.6 mm.

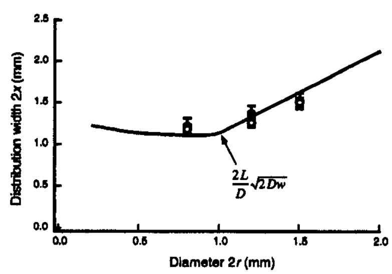

CMD6 Fig. 3 Distribution width ($2x$) vs. object diameter ($2r$). Close circle: experimental data; open circle: Monte Carlo simulation; line: random-phase path integration. D = 12 mm, L = 6 mm, w = 40 μm.

data as well as Monte-Carlo simulations. The three curves agree well. Although multiply scattered paths are too complicated to analyze, the Monte Carlo simulation shows that their contributions are negligible. In Fig. 3, we plot the distribution width vs. the object diameter. The curve shows that there exits a resolution limit $\gamma \approx 2L\sqrt{2Dw/D}$. If the object diameter is larger than γ, the width of the gated-photon distribution approximately equals to the object diameter, otherwise it approximately equals to γ. Our analysis shows that reducing the gate window has only a mild effect on improving the resolution. Because in practice w is limited to about 30 μm (100 fs), for a tissue thickness ≈2 cm, the resolution limit is ≈0.5 mm. Again we have verified our analysis by experiments and Monte Carlo simulations. In Fig. 3 within experimental uncertainties, the data agree with the theoretical curve.

1. H.-P. Chiang, W.-S. Chang, J. Wang, Opt. Lett. **18**, 546 (1993).
2. H.-P. Chiang, J. Wang, in *Conference on Lasers and Electro-Optics*, Vol. 15, 1995 OSA Technical Digest Series (Optical Society of America, Washington, DC, 1995), paper CThI12.

CMD7 **9:45 am**

Optical imaging of phase information through highly scattering media by coherent detection imaging

Shunichi Sato, Noriaki Annaka, Humio Inaba,* *Institute for Advanced Materials Processing, Tohoku University, 2-1-1 Katahira, Aoba-ku, Sendai 980-77, Japan*

Recently, there is a growing number of researches in transillumination imaging through highly scattering media, as a result of the increased interest in optical computed tomography (CT), especially for biomedical applications. Several techniques have been studied[1] to obtain optical images eliminating multiply scattering light. A coherent detection imaging (CDI) method[2-5] can extract only coherent component from the transmitted light on the basis of an optical heterodyne detection technique. So far, amplitude of the heterodyne signal, in other words, the intensity of transmitted coherent light was used to form optical images of scattering or absorption of the objects. However, CDI inherently has a potential to measure phase difference between a signal wave and a reference one, which has information about a refractive index or an optical length of the object.

In this paper, we demonstrate optical imaging of phase information of objects through highly scattering media by using CDI. It is found that this phase imaging is able to obtain information, which is not included in transmitted light intensity.

Figure 1 shows the basic arrangement of the CDI imaging system. This system consists of two Mach-Zehnder interferometers. In the first interferometer, the output beam of a single-frequency He-Ne laser is divided into two, namely a reference beam and a signal beam, with a polarized beam splitter (PBS). Frequency difference of 100 kHz between the two beams is produced by AOMs. After combining the two beams again with another PBS, a part of the beam is used as a reference of phase measurement. Sample is put into one beam of the second interferometer. Because a nonlinear response of PBS generally causes reduction of the dynamic range of the system, the recombined beam is detected by using a balanced detection method. The dynamic range measured is approximately 110 dB and the thermal stability for phase measurement is within 3° per hour.

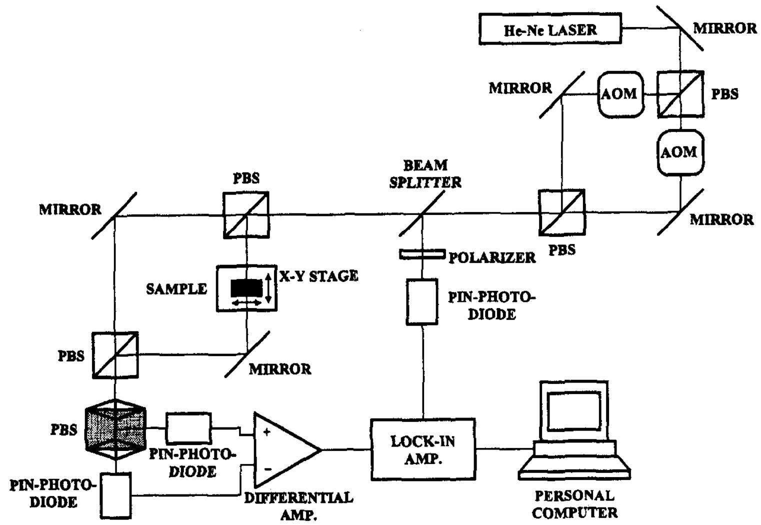

CMD7 **Fig. 1** Schematic diagram of phase imaging system of objects hidden in highly scattering medium.

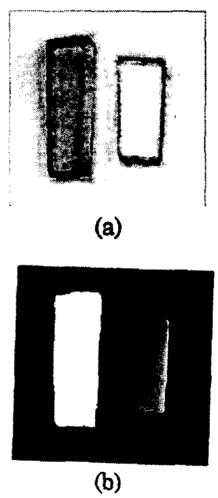

CMD7 **Fig. 2** An example of CDI images of two rectangular color filters held between two scattering plates (left: cyan, right:yelloish). (a) intensity image, (b) phase image. The width of each sample is 2 mm.

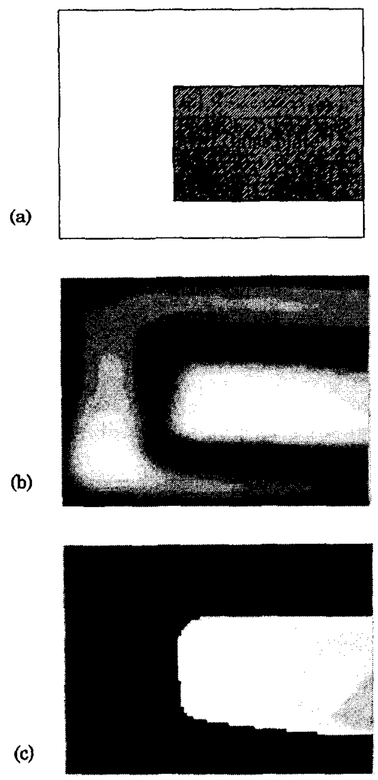

CMD7 **Fig. 3** An example of CDI image of a glass plate suspended in 5% Intralipid scattering medium. (a) the sample position and the shape, (b) intensity image, (c) phase image. The width of the sample is 2 mm.

Figure 2 shows an example of optical images of thin color filters obtained by CDI. Two rectangular filters (left: cyan, right: yellowish) were held between two scattering plates (#800 and #1000). In Fig. 2(a), the portion around the filter edge is dark because the laser light is refracted or scattered more strongly at the edge reducing the intensity of heterodyne signal.